Mathematical Modeling and Algorithm Application
ISSN: 3006-0842 | Vol. 6, No. 1, 2025

Research on Multi Sensor Fault Diagnosis Method Based on Time-Frequency Graph Neural Network

Jinghe Lin*

School of Automation and Electrical Engineering, Lanzhou University of Technology, Lanzhou Gansu 730050, China
* **Corresponding author**: Jinghe Lin (Email: autolin@163.com)

Abstract: With the continuous development of modern industry, numerous sensors have been ubiquitously deployed in industrial systems. Effectively integrating multi-sensor data is of great significance for improving the accuracy and reliability of fault diagnosis. However, most existing methods are limited to a single-level structure and fail to fully exploit the deep-level features within the data, exhibiting notable limitations. To address this issue, this study proposes a fault diagnosis method that integrates time-domain and frequency-domain graph information to more comprehensively extract and utilize fault features from sensor data. Specifically, graph structures in the time and frequency domains are first constructed by analyzing the correlations among different sensors. Then, graph convolutional neural networks are employed to extract features from both types of graphs, while the mutual information between them is minimized to enhance feature independence. Finally, an attention-based fusion strategy is introduced, and a classifier is constructed to improve the reliability of fault diagnosis. Experimental results on the nickel flash smelting furnace system demonstrate that the proposed method achieves a fault diagnosis accuracy exceeding 95.43%, significantly outperforming methods relying solely on time-domain data.

Keywords: Time-Frequency graph neural network; Graph convolutional neural network; Attention mechanism.

1. Introduction

With the rapid development of modern industry, the operational safety of industrial systems has become increasingly critical. During long-term operation, complex and variable production environments and operating conditions can easily lead to various types of equipment failures, which may result in production interruptions or even safety incidents. Therefore, there is a growing urgency for industrial systems to diagnose equipment faults effectively.

Sensors play an increasingly vital role in modern industrial systems, as they comprehensively collect equipment operational status information, providing essential data support for fault diagnosis [1-3]. Effectively integrating and analyzing multi-source sensor information is of great significance for enhancing fault diagnosis capabilities [4]. However, existing studies often rely on a single-layer graph structure during the fusion process, which limits the ability to fully exploit the deep-level features within the data. Traditional methods inadequately capture the complex correlations among multiple sensors and underutilize frequency-domain information, resulting in incomplete fault feature extraction and limited diagnostic reliability in complex industrial environments[5-6].

Traditional fault diagnosis methods typically combine signal processing techniques with machine learning. In the signal processing stage, methods such as Fast Fourier Transform (FFT)[7] and Short-Time Fourier Transform (STFT)[8-9] are commonly used to extract various features from raw data. These approaches often rely on expert experience to manually design feature functions to capture state changes of equipment in both time and frequency domains. These features are then used as inputs to traditional machine learning algorithms[10] to build classification models for identifying fault types. Feng et al. [11] proposed a lightweight fault diagnosis model that improves diagnostic accuracy and robustness by integrating complementary features from time-frequency analysis, followed by optimization and dimensionality reduction. However, such methods have notable limitations: on one hand, the feature extraction process heavily depends on domain expertise and manual intervention, making it subjective and less generalizable; on the other hand, traditional machine learning approaches struggle with representing high-dimensional, nonlinear, and non-stationary signals, making it difficult to effectively handle multi-source heterogeneous signal distributions under complex operating conditions. Consequently, their diagnostic stability in noisy environments or under variable loads is often insufficient.

In recent years, with the rapid advancement of deep learning technologies, Fault diagnosis methods based on data-driven approaches[12] have gradually become a research focus. By constructing multi-layer nonlinear neural networks, these methods enable end-to-end feature learning and condition identification, eliminating the need for tedious and manual feature engineering required in traditional approaches, thereby significantly enhancing the applicability and generalization capability of the models. To further improve the robustness and reliability of diagnostic systems, multimodal sensor fusion techniques[13-14] have attracted growing attention. By integrating multi-source heterogeneous data collected from sensors of different physical properties and locations, the system can obtain more comprehensive and complementary information regarding equipment conditions. Current studies often feed multi-sensor data into deep learning models for joint training and feature fusion, aiming to achieve higher accuracy in fault detection and classification within complex industrial environments.

However, most current research remains confined to single-level or simply concatenated fusion strategies, such as stacking data at the input layer or performing vector concatenation at the feature level. These approaches fall short of fully exploiting the underlying spatiotemporal correlations and semantic complementarity among multi-source signals.

Such shallow fusion mechanisms struggle to effectively reconcile inconsistencies and redundancies across different sensor inputs, and fail to systematically achieve discriminative cross-sensor feature extraction and integration. As a result, their performance improvements in complex industrial environments remain limited.

Accordingly, this study proposes a fault diagnosis method that integrates time-domain and frequency-domain graph information, named the Time-Frequency Graph Fusion Network (TFGFN). First, based on the correlations between different sensor signals, graph structures are constructed in the time domain and frequency domain, respectively. Then, graph convolutional neural networks are used to extract discriminative features from both types of graphs, while the mutual information between features is minimized to enhance their independence. Finally, an attention-based fusion module is introduced to adaptively integrate the dual-domain features, and a classifier is built for fault identification. This framework significantly improves the accuracy and reliability of fault diagnosis.

The remainder of this paper is organized as follows: Section 2 introduces the theoretical foundations of graph convolutional networks and attention mechanisms; Section 3 presents the time-frequency graph neural network and the fault diagnosis model; Section 4 provides experimental validation of the proposed method; Section 5 concludes the paper and summarizes the findings.

2. Theoretical Background

2.1. Graph Convolutional Networks

Graph Convolutional Networks (GCNs), as a significant breakthrough in the field of deep learning for processing non-Euclidean data, provide a powerful framework for representation learning of graph-structured data. Their core idea originates from the concepts of local connectivity and weight sharing in traditional convolutional neural networks, achieving effective aggregation of node neighborhood information through an innovative message-passing mechanism.

The formal definition of a graph in structured data representation is $G=(V,E,A)$, where V denotes the set of nodes and E represents the set of edges. The adjacency matrix $A\in\mathbb{R}^{N\times N}$ quantitatively describes the connectivity between nodes: if node i is connected to node j, then $A_{ij}=1$; otherwise, $A_{ij}=0$. The core propagation mechanism of GCN is implemented through the following formula:

$$Z_{i+1}=\sigma\left(\tilde{D}^{-\frac{1}{2}}\tilde{A}\tilde{D}^{\frac{1}{2}}Z_iW_i\right) \tag{1}$$

where $\tilde{A}=A+I$ represents the adjacency matrix with added self-connections, ensuring that each node retains its own features when aggregating information from neighbors. $\tilde{D}$ is the degree matrix of $\tilde{A}$, satisfying $\tilde{D}_{ii}=\sum_j \tilde{A}_{ij}$, W_i denotes a trainable weight matrix, and $\sigma(\bullet)$ refers to a non-linear activation function. Through this mechanism, each node aggregates feature information from its first-order neighbors. After linear transformation and non-linear activation, higher-level feature representations are generated.

2.2. Attention Mechanism

The attention mechanism draws inspiration from the human ability to selectively focus on critical information. This mechanism dynamically evaluates the importance of different parts of the input and assigns appropriate weights to them, thereby constructing a weighted information representation. By feeding this weighted result into the model, the system can more accurately identify the features most relevant to the task, significantly improving the efficiency of information processing. These weights are typically learned and refined automatically by neural networks in an end-to-end manner.

Assuming the input data and query vector are denoted as $X=\{x_i \mid 1\le i\le N\}$ and Q, the attention score of x_i can be defined as follows:

$$s_i=softmax\left(S\left(x_i,Q\right)\right)=\frac{\exp\left(f\left(d_i,Q\right)\right)}{\sum_{j=1}^{n}\exp\left(f\left(d_j,Q\right)\right)} \tag{2}$$

where $S(\bullet)$ is a scoring function, and $softmax(\bullet)$ converts the scores into a probability distribution, satisfying $\sum_{i=1}^{n}s_i=1$. The weighted sum is then computed using the weights s_i and the corresponding input values d_i, as shown in the following formula:

$$res=\sum_{i=1}^{n}s_id_i \tag{3}$$

Where res represents the key information that the model focuses on.

3. Methodology framework

The Time-Frequency Graph Fusion Network (TFGFN) consists of four key components: a time-domain graph feature extraction module (Time Block), a frequency-domain graph feature extraction module (Frequency Block), a feature fusion module (Fusion Block), and a fault diagnosis module (Detection Block), as illustrated in Fig. 1.

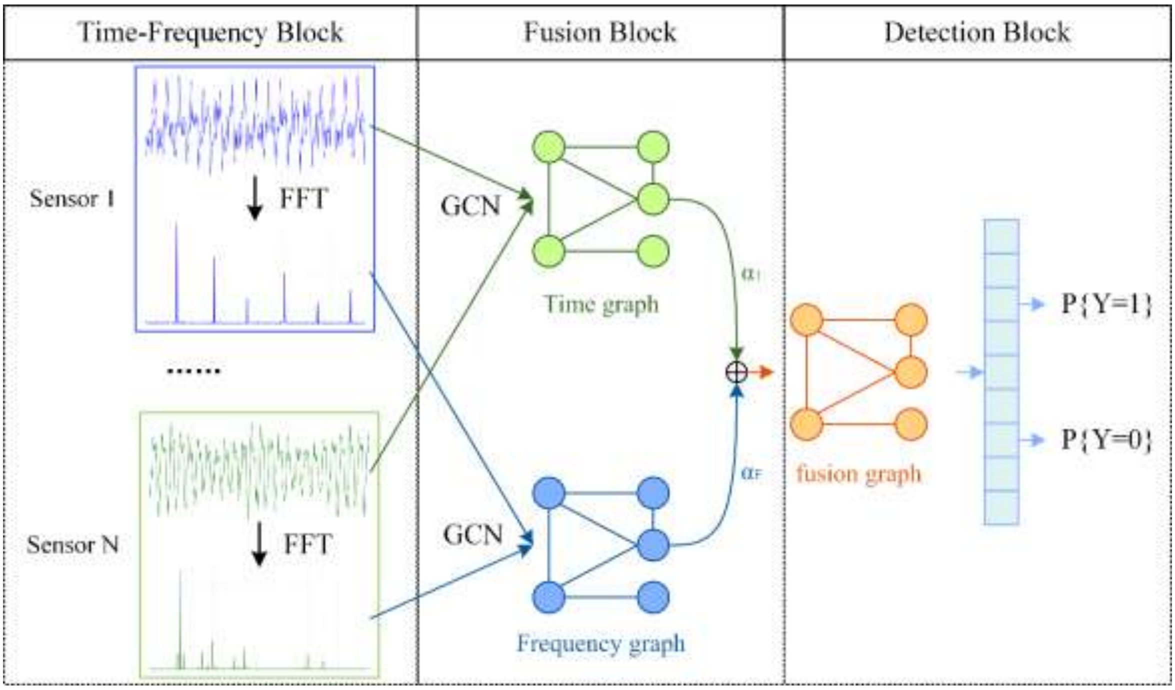

Fig 1. Diagram of the overall framework.

3.1. Time-Frequency domain graph feature extraction module

The core idea of the time-frequency graph feature extraction module lies in collaboratively mining complementary information from time series in both time and frequency domains. Unlike traditional approaches that process time-domain or frequency-domain features in isolation, this module emphasizes joint representation across time and frequency domains, thereby effectively mitigating issues of information fragmentation and underutilization. By introducing a time-frequency mutual information minimization mechanism, the system achieves decoupled representations of time and frequency domains, ultimately extracting more discriminative and less redundant feature representations.

Since frequency domain analysis is required, a Fast Fourier Transform (FFT) must first be applied to convert the time-domain signal from a time-amplitude representation to a frequency-amplitude representation. For a time-domain signal sequence of length N, its frequency-domain representation can be calculated using the formula:

To analyze frequency domain data, a Fast Fourier Transform (FFT) must first be applied to convert the time-domain signal from a time-amplitude representation to a frequency-amplitude representation. For a time-domain signal sequence $T[n]$ of length N, the calculation formula for its frequency-domain representation $F[k]$ is given by:

$$F[k]=\sum_{n=0}^{N-1}T[n]e^{-j\frac{2nk}{N}\pi} \tag{4}$$

Where j is the imaginary unit. The Fast Fourier Transform projects the signal from the time domain to the frequency domain, where each value in $F[k]$ corresponds to a specific frequency component. This clearly reveals the frequency-domain structure of the signal and provides a foundation for subsequent frequency-domain graph construction.

Additionally, to construct edges in the graph structure, mutual information is employed to capture any form of statistical dependency between two variables X and Y. The mutual information can be expressed as:

$$I(X;Y)=\sum_{y\in Y}\sum_{x\in X}p(x,y)\log\left(\frac{p(x,y)}{p(x)p(y)}\right) \tag{5}$$

Where, $p(x,y)$ represents the joint probability distribution of X and Y while $p(x)$ and $p(y)$ denote their marginal probability distributions. Unlike linear correlation coefficients, mutual information can capture nonlinear and non-functional dependencies, making it suitable for modeling implicit couplings among sensors in complex industrial environments. However, since the numerical range of mutual information has no clear upper bound and lacks a unified evaluation criterion, it is difficult to directly compare the association strengths between different node pairs. Therefore, mutual information needs to be normalized into standardized mutual information. After normalization, the association strength acquires a standardized dimension, significantly enhancing the comparability between different variable pairs. The standardized mutual information can be expressed as:

$$NI(X;Y)=\frac{I(X;Y)}{\sqrt{H(X)H(Y)}} \tag{6}$$

Where $H(X)$ and $H(Y)$ represent the entropy of variables X and Y, respectively, expressed as:

$$\begin{cases} H(X)=-\sum_{i=1}^{n}p(x_i)\log(p(x_i)) \\ H(Y)=-\sum_{i=1}^{n}p(y_i)\log(p(y_i)) \end{cases} \tag{7}$$

The value ranges from $NI(X;Y)$ to $[-1,1]$. When $|NI(X;Y)|\le 0.3$, there is no correlation between X and Y.

When $0.3 < |NI(X;Y)| \le 0.5$, there is a weak correlation between X and Y. When $0.5 < |NI(X;Y)| \le 0.7$, there is a strong correlation between X and Y. When $|NI(X;Y)| > 0.7$, there is an extremely strong correlation between X and Y. By setting a threshold τ, when $NI(X;Y) \ge \tau$, it is considered that there exists an association between X and Y; otherwise, it is deemed that there is no association between X and Y.

For multi-sensor collected multivariate time series $S_T = \{t_i \mid 1 \le i \le N\}$, a fixed-length sliding time window can be applied for segmentation. The data from each sensor within each window is treated as a node, and graph structures are constructed from both time-domain and frequency-domain perspectives.

At the time-domain level, the data of each sensor within the time window is used as nodes. Mutual information between sequences is calculated, and a threshold τ_T is set to establish a time-domain graph $G_T = (V_T, E_T, A_T)$, characterizing the statistical dependencies among sensors during the same time period.

In the frequency domain, the multivariate time series S_T is first transformed into a multivariate frequency-domain series $S_F = \{f_i \mid 1 \le i \le N\}$ via Fast Fourier Transform (FFT). Mutual information between frequency-domain sequences is computed, and a threshold τ_F is set to construct a frequency-domain graph $G_F = (V_F, E_F, A_F)$, which identifies potential resonance patterns and frequency-domain correlations among sensors.

After constructing the time-domain graph G_T and the frequency-domain graph G_F, two independent graph convolutional networks f_{G_T} and f_{G_F} can be respectively employed to extract features from the two graph structures, thereby obtaining the corresponding graph-level features Z_T and Z_F, which are expressed as:

$$\begin{cases} Z_T = f_{G_T}\left(G_T; \tilde{A}_T, \tilde{D}_T, W_T\right) = \sigma\left(\tilde{D}_T^{-\frac{1}{2}} \tilde{A}_T \tilde{D}_T^{\frac{1}{2}} G_T W_T\right) \\ Z_F = f_{G_F}\left(G_F; \tilde{A}_F, \tilde{D}_F, W_F\right) = \sigma\left(\tilde{D}_F^{-\frac{1}{2}} \tilde{A}_F \tilde{D}_F^{\frac{1}{2}} G_F W_F\right) \end{cases} \tag{8}$$

To ensure that the features learned from the time-domain and frequency-domain graphs can capture unique information in their respective domains and complement each other, normalized mutual information (NMI) is adopted as a constraint. This minimizes redundancy between temporal and spectral features, thereby facilitating the model's ability to learn more discriminative multi-level features. The loss function can be expressed as:

$$loss_1 = NI(Z_T; Z_F) = \frac{I(Z_T; Z_F)}{\sqrt{H(Z_T) H(Z_F)}} \tag{9}$$

Constraining the correlation between b and c helps prevent the model from learning redundant features, thereby enabling more effective extraction of distinctive characteristics in both the time and frequency domains. This enhances the diversity and robustness of the final embedded representation, which in turn improves the performance and generalization capability of downstream tasks.

Applying a $loss_1$ constraint to penalize the correlation between Z_T and Z_F helps prevent the model from learning redundant features, thereby enabling more effective extraction of distinctive characteristics in both the time and frequency domains. This enhances the diversity and robustness of the final embedded representation, ultimately improving the performance and generalization capability of downstream tasks.

3.2. Time-Frequency domain graph fusion module

After extracting graph-level features Z_T and Z_F from the time and frequency domains respectively, effectively integrating them to construct a unified and highly discriminative representation poses a critical challenge. Time-domain features capture dynamic evolution patterns and localized details of signals along the temporal dimension, such as transient events and trend changes, while frequency-domain features reveal global structural characteristics and periodic patterns in the spectral dimension, such as dominant frequency components and energy distribution. These two types of features differ significantly in physical interpretation and information dimensions, and their respective contributions to downstream tasks often vary depending on the specific sample and data distribution. Therefore, an attention-based adaptive fusion mechanism can be adopted, enabling the model to dynamically assess the importance of time-domain and frequency-domain features and perform weighted integration based on their relevance to the target task.

First, the attention scores corresponding to the features from the two domains are computed separately through an attention network. The attention scores for the temporal feature Z_T and the frequency-domain feature Z_F are denoted as e_T and e_F, respectively, and are expressed as:

$$\begin{cases} e_T = tanh\left(Z_T W_T + b_T\right) V_T \\ e_F = tanh\left(Z_F W_F + b_F\right) V_F \end{cases} \tag{10}$$

Where W_T and W_F are weight matrices, b_T and b_F are bias terms, and V_T and V_F are attention vectors, all of which are learnable parameters.

The raw attention scores e_T and e_F are then normalized into attention weights α_T and α_F using the $softmax$ function, and satisfy $\alpha_T + \alpha_F = 1$. such that as given by:

$$\begin{cases} \alpha_T = \dfrac{\exp(e_T)}{\exp(e_T) + \exp(e_F)} \\ \alpha_F = \dfrac{\exp(e_F)}{\exp(e_T) + \exp(e_F)} \end{cases} \tag{11}$$

Finally, the temporal and frequency-domain features are fused based on the attention weights to obtain a comprehensive representation Z_{all} This approach preserves the complementary nature of time-frequency information while emphasizing the more critical components through the attention mechanism. The fusion process can be expressed as:

$$Z_{all} = \alpha_T Z_T + \alpha_F Z_F \tag{12}$$

3.3. Classifier

To achieve accurate industrial equipment fault diagnosis, this paper proposes a deep learning-based classifier that takes multi-dimensional fused features as input. These features are efficiently processed by a feedforward neural network incorporating regularization terms, ultimately outputting a probability distribution indicating fault versus normal conditions. To address the common issue of class imbalance in industrial data, a weighted cross-entropy loss function is adopted, significantly enhancing the recognition capability and sensitivity towards minority classes.

First, the input feature Z_{all} is projected into a hidden space via a fully connected layer, and nonlinearity is introduced using the $ReLu$ activation function to enhance the model's expressive capacity. To further improve generalization and alleviate overfitting, $Dropout$ regularization is applied, where during forward propagation, neurons in the hidden layer are randomly dropped with probability $p = 0.1$, thereby effectively suppressing co-adaptation among neurons. The resulting regularized hidden feature h is obtained as:

$$h = Dropout\left(ReLu\left(W_h Z_{all} + b_h\right), p = 0.1\right) \tag{13}$$

Where, W_h denotes the weight matrix and b_h the bias vector, both of which are learnable parameters.

The regularized hidden feature h is then fed into a linear output layer and normalized via the $softmax$ function to produce a probability distribution over the two classes:

$$\begin{cases} P\{Y=0\} = \dfrac{\exp\left(W_{21}h\right)}{\exp\left(W_{21}h\right) + \exp\left(W_{22}h\right)} \\ P\{Y=1\} = \dfrac{\exp\left(W_{22}h\right)}{\exp\left(W_{21}h\right) + \exp\left(W_{22}h\right)} \end{cases} \tag{14}$$

Where, W_{21} and W_{22} represent the weight matrices, $Y = 1$ denotes the "normal state", and $Y = 0$ indicates the "fault state". The resulting probability output clearly reflects the model's confidence level regarding the sample's membership in each class. If $P\{Y=1\} > P\{Y=0\}$ the sample is classified as normal with the predicted label $\hat{Y} = 0$. otherwise, it is classified as faulty with $\hat{Y} = 1$.

Due to the class imbalance commonly encountered in industrial scenarios—where normal samples significantly outnumber fault samples—model training can become dominated by the majority class, leading to notably reduced recognition performance for the minority class. To mitigate this issue, a weighted cross-entropy loss function is employed as the classification loss. By assigning different weights to samples from different classes, this loss significantly enhances the model's sensitivity to rare fault samples, thereby improving its ability to accurately identify fault conditions. The weighted cross-entropy loss is defined as follows:

$$loss_2 = -\frac{1}{N}\sum_{i=0}^{N-1}\left(w_0 Y_i \log P\{Y_i = 0\} + w_1\left(1 - Y_i\right)\log P\{Y_i = 1\}\right) \tag{15}$$

Where, N is the number of samples, $Y_i \in \{0,1\}$ represents the ground truth label of the i sample, $P\{Y_i = 0\}$ and $P\{Y_i = 1\}$ denote the predicted probabilities of the sample being normal and faulty, respectively, and w_0 and w_1 are the class weight coefficients. These coefficients are determined by the number of samples in the training set and are defined as:

$$\begin{cases} w_0 = \dfrac{N_{normal} + N_{fault}}{2N_{normal}} \\ w_1 = \dfrac{N_{normal} + N_{fault}}{2N_{fault}} \end{cases} \tag{16}$$

Where, N_{normal} and N_{fault} represent the number of normal-state samples and fault-state samples in the training set, respectively. During the end-to-end training process, a multi-objective joint optimization loss is constructed to simultaneously achieve two key objectives: the model learns to minimize the correlation between time-domain and frequency-domain feature representations by reducing the correlation loss $loss_1$ thereby enhancing the diversity and complementarity of the features, whereas it also ensures high classification accuracy by minimizing the classification loss $loss_2$ to improve predictive performance. The overall loss function is formed by combining these two losses through weighted summation:

$$loos = \mu_1 loss_1 + \mu_2 loss_2 \tag{17}$$

Where, μ_1 and μ_2 are weighting coefficients that balance the contributions of the two loss terms to the overall objective. This joint loss function guides the model to simultaneously optimize both the feature extraction module and the classifier module during training. Throughout backpropagation, gradients are derived from both the correlation loss and the classification loss, enabling parameter updates under the joint guidance of the two objectives. This design not only prevents the feature representations from converging to a local optimum dominated by a single objective but also enhances the model's generalization capability and robustness, leading to improved performance in complex tasks.

4. Experimental Verification

4.1. Dataset

The data used in this study were obtained from a nickel flash smelting furnace system at a nickel smelter. This system processes nickel concentrate through the flash furnace to produce low nickel matte, simultaneously generating nickel smelting slag. The process flow of the nickel flash smelting furnace system is shown in Fig. 2. To address the issues of prediction and fault diagnosis for sensor data in the flash smelting furnace system, this study selected eight representative sensors under three working conditions for simulation and validation. The monitored parameters cover key indicators such as temperature, pressure, and vibration. Each working condition includes 10 datasets: one set of normal data (100000 samples) and nine sets of fault data (1500 samples each). All data were randomly stratified and split, with 80% used for model training and 20% for testing. Detailed information of the selected sensors is provided in Table 1.

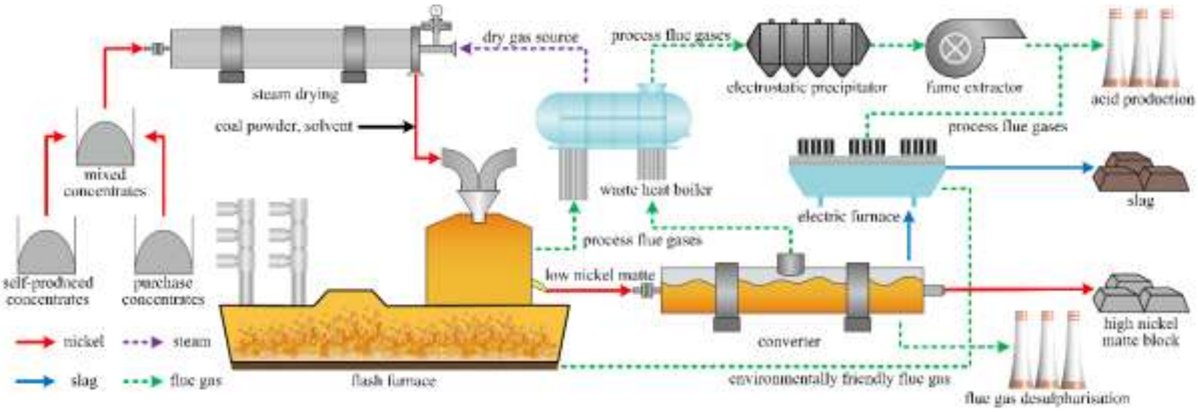

Fig 2. Nickel flash smelting process flow diagram.

Table 1: sensor information.

serial number	sensor	description
X_1	FF-LD-WD-1	Temperature of furnace bottom thermocouple 1
X_2	FF-LD-WD-2	Temperature of furnace bottom thermocouple 2
X_3	FF-LD-WD-3	Temperature of furnace bottom thermocouple 3
X_4	EF-LN-FY-1	Electric furnace negative pressure 1
X_5	EF-LN-FY-2	Electric furnace negative pressure 2
X_6	EF-LN-FY-3	Electric furnace negative pressure 3
X_7	FF-LT-ZD-1	Furnace vibration 1
X_8	FF-LT-ZD-2	Furnace vibration 2

The precise placement and functional configuration of sensors are of critical importance, as they not only provide comprehensive coverage of key monitoring areas in the flash smelting furnace system but also establish a solid foundation for high-quality data acquisition and in-depth analysis. Leveraging data obtained from multi-source sensors, it is possible to conduct thorough analyses of equipment operating conditions and achieve accurate predictions of potential faults. Therefore, by employing multi-sensor data fusion analysis, fault risks in the flash smelting furnace system can be effectively identified and assessed, which is of significant importance for enhancing operational efficiency and ensuring production safety.

4.2. Normalized mutual information

The precise placement and functional configuration of sensors in the flash furnace system form the critical foundation for establishing a comprehensive monitoring system and achieving efficient data acquisition. To thoroughly evaluate the correlation and independence among various sensor signals, this study takes the data from eight sensors under three working conditions as the research subject and calculates the average normalized mutual information matrix among the data of these eight sensors, as shown in Fig. 3- Fig. 4.

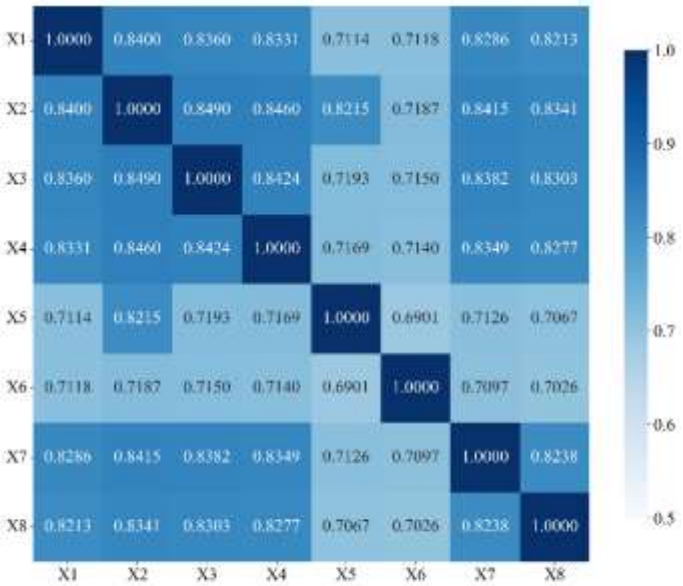

Fig 3. Time domain normalized mutual information matrix.

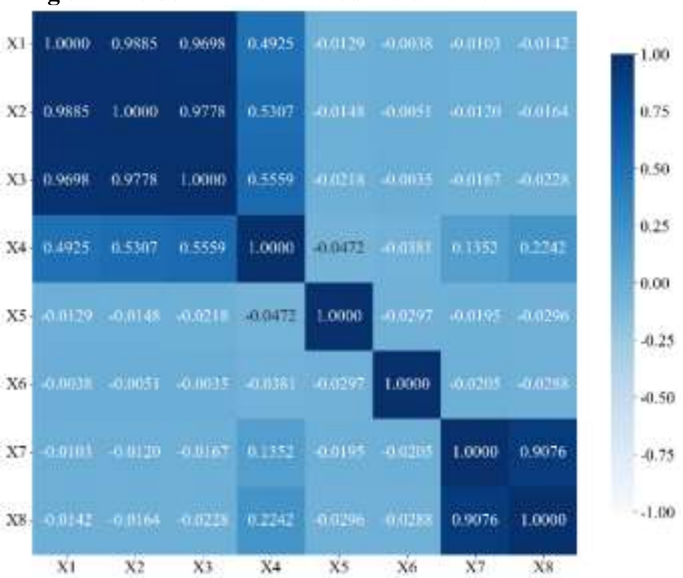

Fig 4. Frequency domain normalized mutual information matrix.

Fig. 3 shows the normalized mutual information matrix between the time-domain data of the sensors. This matrix objectively reflects the statistical dependency degree of the monitoring data from the eight sensors in the time domain. The diagonal elements of the matrix are all 1, indicating that each sensor is completely correlated with itself. The off-diagonal elements quantify the correlation strength between different sensors, with a value range of [0,1]. A higher value indicates a stronger statistical dependency. For instance, there is a high dependency between X_1 and X_2 (0.8400), while the dependency between X_5 and X_6 is relatively low (0.6901). This matrix provides direct data support for constructing a time-domain graph. Specifically, the eight sensors are treated as nodes, and edges are drawn between two sensor nodes whose mutual information value exceeds 0.7, thereby constructing a time-domain graph that effectively characterizes the associative topology of the sensor network in the time domain.

Fig. 4 shows the correlation coefficient matrix between the frequency-domain data of the sensors, which objectively reflects the degree of linear correlation among the monitoring data from the eight sensors in the frequency domain. The diagonal elements of the matrix are all 1, indicating that each sensor is perfectly correlated with itself. The off-diagonal elements quantify the strength of the linear correlation between different sensor pairs, with values ranging from [-1, 1]. Positive values indicate a positive correlation, negative values indicate a negative correlation, and the absolute value reflects the strength of the linear relationship. The matrix reveals extremely strong positive correlations among X_1, X_2, and X_3 (ranging from 0.9698 to 0.9885), a high correlation between X_7 and X_8 (0.9076), while X_5 and X_6 exhibit very weak correlations with other sensors. This matrix serves as the basis for constructing a frequency-domain graph, where the eight sensors are treated as nodes, and edges are drawn between any two sensor nodes whose correlation coefficient absolute value exceeds 0.5. This graph effectively characterizes the associative topology of the sensor network in the frequency domain.

In summary, Fig. 3 shows the normalized mutual information matrix for the sensor time-domain data, while Fig. 4 shows the normalized mutual information matrix for the sensor frequency-domain data. These two matrices objectively reflect the statistical dependencies among the monitoring data from different sensors in the time and frequency domains, respectively. They provide a critical data-driven foundation for constructing both the time-domain and frequency-domain graphs.

4.3. Weight coefficient

A dual-optimizer configuration was adopted, with the learning rate for weight coefficients set to 0.005 and that for the remaining parameters set to 0.001. The updating process of the weight coefficients is illustrated in Fig. 5. To eliminate the influence of initial values on the convergence results, the model was trained under multiple initial conditions. Although the weight coefficients did not fully stabilize at a fixed value in each training round, their convergence error range decreased progressively, and the final fluctuations were controlled within a narrow margin.

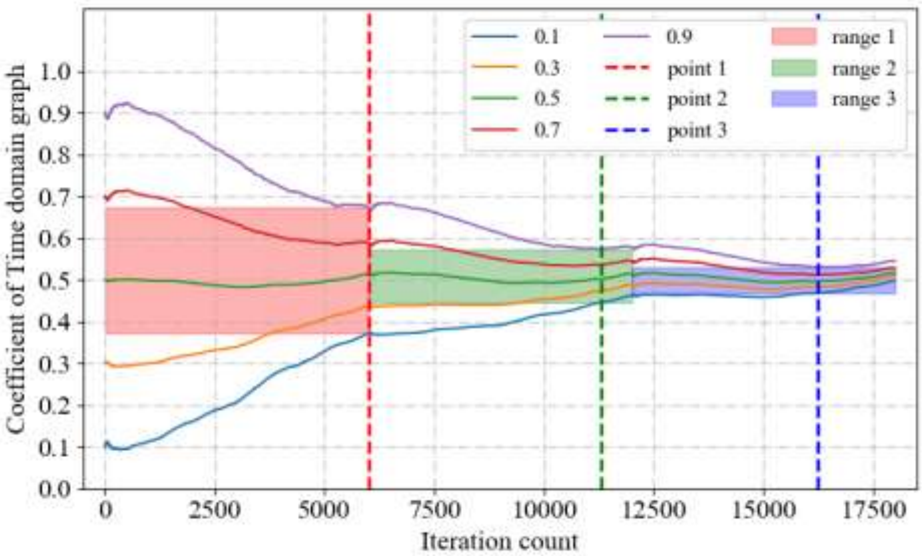

Fig 5. Update curve for the time-domain graph proportion coefficient.

Therefore, the lowest point before the rise of the weight coefficients in each training round was selected as the optimal value for that round, and the average of these optimal values across all rounds was taken as the final selection of the weight coefficient. The optimal selection result is shown in Table 2, where the weight coefficient for the time-domain graph is set to 0.4976.

Table 2: Weight coefficient update data.

Round	Error interval	Range of error	Coefficient
1	[0.3722,0.6738]	0.3016	0.5170
2	[0.4457,0.5728]	0.1271	0.5059
2	[0.4681,0.5300]	0.0619	0.4976

4.4. Comparative experiment

Based on time-domain and frequency-domain features derived from equipment monitoring data, this approach integrates the strengths of both feature types to enable comprehensive analysis and achieve accurate fault diagnosis. To thoroughly evaluate the performance of the proposed fault prediction method, the following classification metrics are employed to assess its effectiveness in fault identification.

Accuracy:

$$ACC = \frac{TP+TN}{TP+FP+TN+FN} \tag{18}$$

Precision:

$$PRE = \frac{TP}{TP+FP} \tag{19}$$

Recall:

$$REC = \frac{TP}{TP+FN} \tag{20}$$

F1-Score:

$$\mathrm{F1} = 2\times\frac{PRE\times REC}{PRE+REC} \tag{21}$$

Where, TP represents the number of samples correctly predicted as positive by the model. TN represents the number of samples correctly predicted as negative by the model. FP represents the number of samples incorrectly predicted as positive by the model. FN represents the number of samples incorrectly predicted as negative by the model.

To clearly demonstrate the advantages of combining time-domain and frequency-domain features, the following two sets of experiments were designed for comparison, highlighting the benefits of the time-frequency representation.

a) Experimental Group 1: Combined time-domain and frequency-domain features;

b) Experimental Group 2: Time-domain features only.

The fault diagnosis performance of the equipment was evaluated using the two experimental groups. The classification metrics are presented in Table 3, and the confusion matrix of the classification results is shown in Fig. 6, which visually reflects the correct classifications and misjudgments under three different operating conditions.

Table 3: Fault prediction evaluation indicators.

Experimental Group	operating condition	ACC	PRE	REC	F1
1	1	98.78%	99.79%	89.23%	0.942
1	2	97.89%	97.37%	84.02%	0.902
1	3	98.12%	95.52%	86.98%	0.911
2	1	68.82%	36.01%	12.69%	0.188
2	2	63.41%	32.46%	9.81%	0.151
2	3	63.33%	30.02%	9.19%	0.141

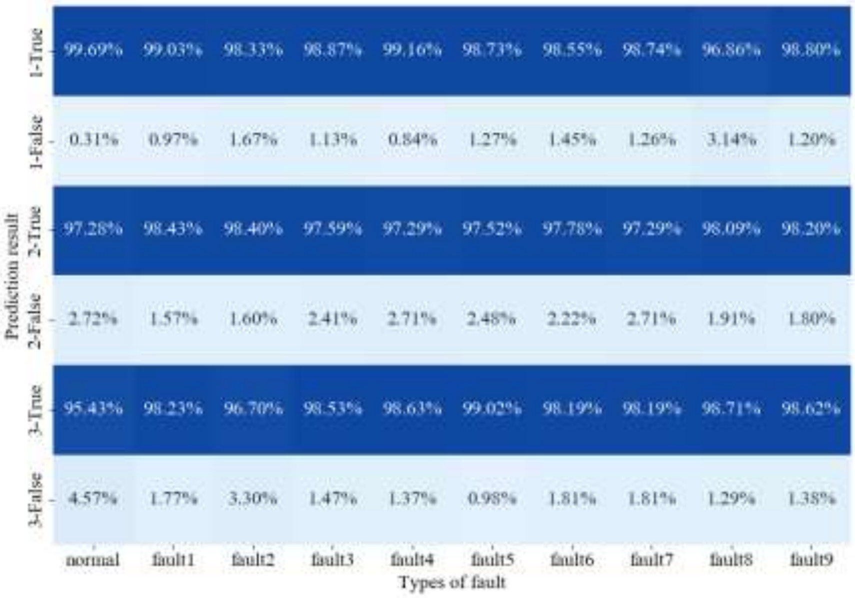

(a) Experimental Group 1: prediction results under three operating conditions

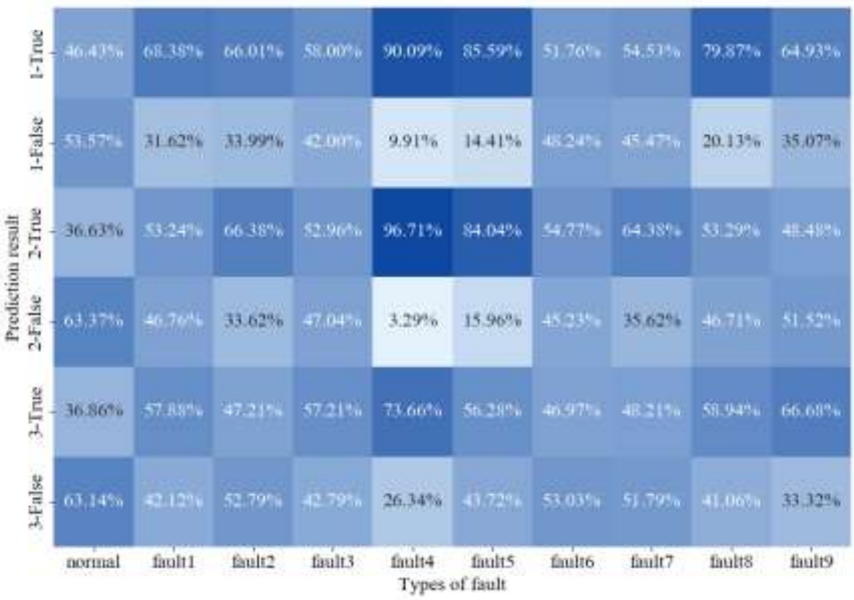

(b) Experimental Group 2: prediction results under three operating conditions.

Fig 6. Fault prediction results.

Through a comparative analysis of the performance between two experimental models, it was observed that when relying exclusively on time-domain data, the model achieved an accuracy of 96.71% in detecting Fault 4, yet its overall performance demonstrated considerable instability, with the detection accuracy for Fault 6 being only 46.97%. More importantly, the model has a high misclassification rate of 63.99% for normal samples, significantly undermining its practical applicability. In contrast, the model incorporating both time-domain and frequency-domain features displayed notable advantages. Experimental results indicate that this model consistently achieved detection accuracy above 95% for all fault types, while maintaining a false positive rate below 4.5% and a false negative rate no higher than 3.2%. This superior performance can be attributed to its innovative architecture, which enhances both detection sensitivity and stability. It is noteworthy, however, that room for improvement remains in the model's ability to correctly identify normal samples, thus providing a clear direction for future research.

5. Summary

This study proposes a fault diagnosis method that integrates time-domain and frequency-domain graph information, aiming to more comprehensively extract and utilize fault features from sensor data. Specifically, graph structures in the time and frequency domains are first constructed based on correlation analysis among different sensors. Subsequently, graph convolutional networks are employed to extract features from both types of graphs, while the mutual information between them is minimized to enhance feature independence. Finally, an attention-based fusion strategy is introduced, and a classifier is constructed to effectively improve the accuracy and reliability of fault diagnosis.

Acknowledgments

This work was supported by the National Natural Science Foundation of China (62263020), the Key Project of Natural Science Foundation of Gansu Province (25JRRA061), the Major Project of Gansu Province Joint Research Fund (25JRRA1144), the Key R&D Program of Gansu Province (23YFGA0061), and the Hongliu Outstanding Young Talents Support Project of Lanzhou University of Technology.

References

[1] Lei L, Li W, Zhang S, et al. Research Progress on Data-Driven Industrial Fault Diagnosis Methods. SENSORS,Vol 25, pp. 2952-2952, 2025.

[2] Jia T, Tian Y, Yin Z, et al. Data-free stealing attack and defense strategy for industrial fault diagnosis system. Chemical Engineering Research and Design, Vol 216, pp. 200-215, 2025.

[3] Lin J, Ren G, Huang K, et al. A novel multi-sensor information fusion method for fault diagnosis of rotating machinery with missing signals. Advanced Engineering Informatics, Vol 68, pp. 103595, 2025.

[4] Carlos F, David D, Jose L, et al. Fuzzy processing applied to improve multimodal sensor data fusion to discover frequent behavioral patterns for smart healthcare. Information Fusion, Vol 123, pp. 103307, 2025.

[5] Deng X, Wang Y, Yang W. A sensitive efficient multiple predictable feature extraction and fusion method for complicated industrial fault detection. CHEMOMETRICS AND INTELLIGENT LABORATORY SYSTEMS,Vol 263, 2025.

[6] Zhu D, Liu G, He W, et al. Fault feature extraction of rolling element bearing based on EVMD. JOURNAL OF THE BRAZILIAN SOCIETY OF MECHANICAL SCIENCES AND ENGINEERING,Vol 43, pp. 1-14, 2021.

[7] Lee C, Le T. Intelligence Bearing Fault Diagnosis Model Using Multiple Feature Extraction and Binary Particle Swarm Optimization With Extended Memory. IEEE ACCESS, Vol 8, pp. 198343-198356, 2020.

[8] Ribeiro J, Ronny F, Santos A, et al. Fault Detection and Diagnosis in Electric Motors Using Convolution Neural Network and Short-Time Fourier Transform. JOURNAL OF VIBRATION ENGINEERING & TECHNOLOGIES, Vol 10, pp. 2531-2542, 2022.

[9] Xiang G, Miao G, Cui L, et al. Intelligent Fault Diagnosis for Inertial Measurement Unit through Deep Residual Convolutional Neural Network and Short-Time Fourier Transform. MACHINES, Vol 10, pp. 851, 2022.

[10] Feng T, Wang Z, Qiu L, et al. Rolling Based on Multi-Source Time-Frequency Feature Fusion with a Wavelet-Convolution, Channel-Attention-Residual Network-Bearing Fault Diagnosis Method. SENSORS, Vol 25, pp. 4091, 2025.

[11] Sun C, Wang Y, Tian Z, et al. Optimal symplectic geometric bi-spectrum mutual information contrastive learning framework for fault diagnosis of helicopter spiral bevel gear. MEASUREMENT SCIENCE AND TECHNOLOGY, Vol 36, pp. 066004-066004, 2025.

[12] Lei L, Li W, Zhang S, et al. Research Progress on Data-Driven Industrial Fault Diagnosis Methods. SENSORS, Vol 25, pp. 2952-2952, 2025.

[13] Ma L, Peng K, Yang Q. A unified representation and fusion framework of multi-source heterogeneous data for fault diagnosis in industrial processes. ADVANCED ENGINEERING INFORMATICS, Vol 67, 2025.

[14] Ma L, Yang Q, Long Z, et al. A multi-source heterogeneous data fusion framework for fault diagnosis in industrial processes with missing image data. MEASUREMENT, Vol 256, 2025.